A Method of Reduced-Order Modal Computation for Planning Grid Connection of a Large-Scale Wind Farm

Wenjuan Du, *Member, IEEE*, Wenkai Dong, and Haifeng Wang, *Senior Member, IEEE*

***Abstract*—For planning the grid connection of a wind farm, small-signal stability needs to be examined to ensure the stability of wind farm as a standalone system. However, for a large-scale wind farm with *m* wind turbine generators (WTGs), the dimension of state matrix is *nm* if on average the order of dynamic models of the WTGs is *n*. Thus, when the number of the WTGs in the wind farm is over several hundred or more, high-dimensional numerical difficulty of modal computation may occur. Therefore, in this paper, we propose a method of reduced-order modal computation for the application in planning the grid connection of the large-scale wind farm. Dimensions of matrices involved in the reduced-order modal computation are *m* and *n* such that the numerical difficulty of modal computation is effectively avoided. In the paper, the effectiveness of proposed method of reduced-order modal computation is demonstrated and evaluated by an illustrative simple example wind farm and an example large-scale wind farm with 200 WTGs.**

***Index Terms*—Small-signal stability of wind farm, reduced-order modal computation, similarity of matrix.**

NOMENCLATURE

$\mathbf{A}_p$	State matrix of an individual WTG in a wind farm.
$\mathbf{B}_p$	Control matrix of the WTG in the wind farm.
$\mathbf{C}_p$	Output matrix of the WTG in the wind farm.
$\mathbf{A}_w$	State matrix of the wind farm.
$\mathbf{B}_w$	Control matrix of the wind farm.
$\mathbf{C}_w$	Output matrix of the wind farm.
$\Delta\mathbf{X}_k$	Vector of all the state variables of the *k*th WTG in the wind farm.
$\Delta\mathbf{X}_w$	Vector of all the state variables of the wind farm.
$\mathbf{C}_{w3}$	Structure matrix of a wind farm with three WTGs.
$\mathbf{C}_{wm}$	Structure matrix of the wind farm with *m* WTGs.
λ_k	The *k*th eigenvalue of structure matrix of the wind farm.
$\mathbf{P}_3$	Similarity transformation matrix for $\mathbf{C}_3$.
$\mathbf{P}_m$	Similarity transformation matrix for $\mathbf{C}_m$.
$V_{kx}+jV_{ky}$	Terminal voltage of the *k*th WTG in the wind farm.
$I_{kx}+jI_{ky}$	Output current of the *k*th WTG in the wind farm.
R_c+jX_c	Impedance/per km of the cable in the wind farm.
l_{ij}	Length of cable connecting the *i*th and *j*th WTG.
m	Number of WTGs in the wind farm.
n	Order of dynamic model of an individual WTG.
Full-order model	Model of a wind farm with *m* WTGs. Dimension of the model is *mn*.
Planning model	Model of the wind farm, where dynamic models of *m* individual WTGs are identical.
Similar model	Model of the wind farm, state matrix of which is a block diagonal matrix and similar to that of planning model. Dimension of the model is *mn*.
Structure matrix	A matrix determined by the topology of wind farm network. Dimension of structure matrix is *m*.
CMV method	Capacity-weighted mean value method.
PI method	Parameter identification method.

Manuscript received November 2, 2018; revised March 19, 2019; accepted April 29, 2019. Date of publication June 3, 2019; date of current version June 19, 2020. This work was supported by the State Grid Corporation of China under Grant NYB17201800102. Paper no. TSTE-01095-2018. *(Corresponding author: Haifeng Wang.)*

W. Du is with the School of Electrical Engineering, Sichuan University, Chengdu 610017, China (e-mail: ddwenjuan@qq.com).

W. Dong and H. Wang are with the State Key Laboratory of Alternate Electric Power Systems With New Energy Resources, North China Electric Power University, Beijing 102206, China (e-mail: 596167281@qq.com; hfwang60@qq.com).

Color versions of one or more of the figures in this paper are available online at http://ieeexplore.ieee.org.

Digital Object Identifier 10.1109/TSTE.2019.2920409

I. INTRODUCTION

A LARGE-SCALE wind farm may be comprised of several hundreds of wind turbine generators (WTGs). Dynamic interactions among the WTGs in the wind farm and between the wind farm and the grid are very complicated. Hence, it has been an important and challenging task to plan the grid connection of such large-scale wind farm with the dynamic characteristics of the wind farm being considered [1]–[3]. One essential issue is the small-signal stability of the wind farm and the power system affected by the grid connection of the wind farm. The issue must be considered and assessed carefully at the stage of planning the grid connection of the wind farm.

For the assessment of impact of grid-connected wind farm on the small-signal stability of power system, normally the reduced-order model of wind farm has been used, which is represented as one or several aggregated WTGs. Utilization of reduced-order model simplifies the assessment and is effective to identify any instability risk of the external power system which may be brought about by the grid connection of the wind farm [4]–[9]. So far, two main categories of methods to develop the reduced-order model of the wind farm have been proposed. They are the capacity-weighted mean value (CMV) method and the parameter identification (PI) method.

The CMV method uses the ratios of rated capacities of individual WTGs to the total capacity of wind farm as the weights. Reduced-order model of the wind farm is obtained as an aggregated WTG with the parameters being calculated from the weighted parameters of individual WTGs in the wind farm [10]–[12]. The CMV method is computationally simple and has been widely adopted in planning the grid connection of wind farm. The reduced-order model derived by the CMV method stands when the operating conditions of wind farm vary. However, the CMV method mainly considers the equivalence of generating capability of wind farm to that of aggregated WTG. The wind farm topology is represented simply by a single equivalent impedance in the reduced-order model. Impact of wind farm's topology on the stability of wind farm is not fully represented in the reduced-order model.

PI method is to match the dynamics between the wind farm and its aggregation. The reduced-order model is obtained by minimizing the difference of the dynamics [13]–[16]. PI method can fully consider the impact of wind farm's topology. However, it is sensitive to the variation of operating conditions of wind farm. When the wind conditions vary, different results of reduced-order model may be obtained.

When the grid connection of a wind farm is planned, the small-signal stability of wind farm needs to be assessed to ensure that the wind farm is stable as a standalone system. For the assessment, detailed models of WTGs in the wind farm can be used to establish the full-order dynamic model of the wind farm [17], [18]. However, when the number of WTGs in the wind farm is considerable, dimension of state matrix of the wind farm can be very high. Subsequently, numerical difficulty of modal computation of high-dimensional state matrix may occur. To avoid the numerical difficulty, a reduced-order model of wind farm can be derived. However, at planning stage, impact of wind farm topology and variation of operating conditions of wind farm are often two important factors which need to be examined comprehensively. Both the CMV method and PI method need to be improved for the examination due to the weakness of CMV method in considering the impact of wind farm topology and the sensitivity of PI method to the variation of operating conditions of the wind farm.

In this paper, a reduced-order method of modal computation is proposed for assessing the stability of a wind farm with m WTGs for planning the grid connection of the wind farm. A structure matrix is proposed to represent the topology of the wind farm. Dimension of the structure matrix is m. At the planning stage, typical model, parameters and operating conditions are normally used for all the WTGs in the wind farm. Hence, it can be assumed that the dynamic models of m WTGs are identical. Under this assumption, full-order state-space model of the wind farm is derived. Mathematical proof is presented in the paper to indicate that the full-order state matrix can be decomposed to a block diagonal matrix by using the similarity transformation. There are m diagonal matrices in the block diagonal matrix. Dimension of each of m diagonal matrices is n, which is the order of dynamic model of an individual WTG in the wind farm. Each of m diagonal matrices can be established by using the state-space model of the individual WTG and an eigenvalue of structure matrix. Hence, the mathematical proof shows that the wind farm can be equivalently decomposed to m dynamically independent subsystems. State matrices of the subsystems are the diagonal matrices of the block diagonal matrix obtained via the similarity transformation. Therefore, it is proposed that the stability of the wind farm being planned for the grid connection is assessed by the results of modal computation of m subsystems. Dimension of full-order state matrix is nm. Dimension of structure matrix is m and that of the state matrix of a subsystem is n. Hence, the method of modal computation proposed is reduced-order.

Mathematical derivation presented in the paper focuses on proving that the wind farm can be represented by m dynamically independent reduced-order subsystems, rather than establishing a reduced-order model of the wind farm. The reduced-order method of modal computation is based on the equivalence between the full-order state matrix and state matrices of subsystems. The equivalence is established by considering the wind farm topology represented by the structure matrix and stands when the operating conditions of wind farm vary. Hence, it overcomes the drawbacks of stability assessment by using the reduced-order model of wind farm obtained by either the CMV method or the PI method. The paper is organized as follows.

In the next section, an illustrative simple example wind farm with three WTGs is presented. Firstly, full-order model of the example wind farm is derived. Secondly, a planning model is established when the dynamic models of three WTGs are assumed to be identical for planning the grid connection of the wind farm. In the derivation, a structure matrix of the wind farm is introduced. Dimension of structure matrix is 3, the number of WTGs in the wind farm. Secondly, similarity transformation is introduced and taken to the state matrix of planning model of the wind farm. Result of similarity transformation indicates that the state matrix of planning model can be equivalently transformed to a block diagonal matrix. Thus, stability of the wind farm can be assessed by the modal computation from the three diagonal matrices.

In Section III, the decomposition of full-order model is extended and proved to the case of general wind farm with m WTGs. The reduced-order method of modal computation is proposed to assess the stability of the wind farm being planned for the grid connection.

In Section IV, a simple numerical example of wind farm with three PMSGs is presented to demonstrate how the proposed method of reduced-order modal computation is applied to assess the stability of wind farm. In the section, a simple case of application is firstly demonstrated for the tutorial purpose. Then,

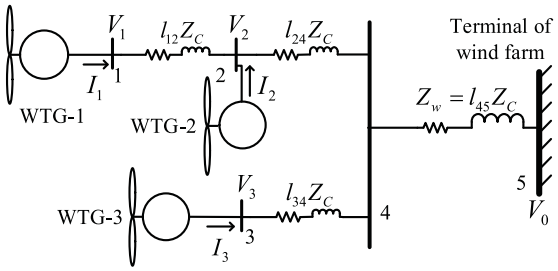

Fig. 1. Configuration of an illustrative simple example wind farm.

a case is presented when the detailed 15th -order model of PMSG is used.

In Section V, a large-scale wind farm with 200 PMSGs is presented. The reduced-order method of modal computation proposed in the paper is validated and compared with the widely-used CMV method for the following factors which are usually the main concerns in planning the grid connection of wind farm: (1) Geographical area occupied by the wind farm; (2) Selection of typical parameters of WTGs; (3) Variations of parameters and loading conditions of PMSGs in the wind farm.

Final section summarizes the conclusions of the paper.

II. An Illustrative Simple Wind Farm With Three WTGs

A. Full-Order State-Space Model of a Wind Farm

In order to clearly introduce the method of reduced-order modal computation to be proposed, an illustrative simple wind farm with three WTGs is presented in this section. Three WTGs are arranged in two strings as shown by Fig. 1. In the first string, there are two WTGs and in the second string, there is only one WTG. In Fig. 1, $Z_C = R_C + jX_C$ is the impedance of cable/per km inside the wind farm; l_{12}, l_{24}, l_{34} and l_{45} is the length of each section of cable (in km.) between node 1, 2, 3, 4 and 5. For the stability assessment of standalone wind farm, voltage at node 5 (terminal of wind farm) can be assumed to be constant.

From Fig. 1, following linearized voltage equations can be obtained

$$\begin{aligned}\Delta \boldsymbol{V}_1 &= l_{12}\boldsymbol{Z}_C\Delta \boldsymbol{I}_1 + l_{24}\boldsymbol{Z}_C\left(\Delta \boldsymbol{I}_1+\Delta \boldsymbol{I}_2\right)\\ &\quad + l_{45}\boldsymbol{Z}_C\left(\Delta \boldsymbol{I}_1+\Delta \boldsymbol{I}_2+\Delta \boldsymbol{I}_3\right)\\ \Delta \boldsymbol{V}_2 &= l_{24}\boldsymbol{Z}_C\left(\Delta \boldsymbol{I}_1+\Delta \boldsymbol{I}_2\right) + l_{45}\boldsymbol{Z}_C\left(\Delta \boldsymbol{I}_1+\Delta \boldsymbol{I}_2+\Delta \boldsymbol{I}_3\right)\\ \Delta \boldsymbol{V}_3 &= l_{34}\boldsymbol{Z}_C\Delta \boldsymbol{I}_3 + l_{45}\boldsymbol{Z}_C\left(\Delta \boldsymbol{I}_1+\Delta \boldsymbol{I}_2+\Delta \boldsymbol{I}_3\right)\end{aligned} \tag{1}$$

where $\Delta \boldsymbol{I}_k = [\,\Delta I_{kx}\ \Delta I_{ky}\,]^T$ and $\Delta \boldsymbol{V}_k = [\,\Delta V_{kx}\ \Delta V_{ky}\,]^T$; $V_{kx} + jV_{ky}$ and $I_{kx} + jI_{ky}$, $k = 1, 2, 3$ are the terminal voltage and output current of the kth WTG respectively, expressed in the common $x - y$ coordinate of the wind farm, $\boldsymbol{Z}_C = \left[\begin{smallmatrix} R_C & -X_C \\ X_C & R_C \end{smallmatrix}\right]$.

Let the state-space model of the kth WTG in the wind farm be

$$\begin{aligned}\frac{d}{dt}\Delta \boldsymbol{X}_k &= \boldsymbol{A}_k\Delta \boldsymbol{X}_k + \boldsymbol{B}_k\Delta \boldsymbol{V}_k\\ \Delta \boldsymbol{I}_k &= \boldsymbol{C}_k\Delta \boldsymbol{X}_k,\ \ k = 1, 2, 3\end{aligned} \tag{2}$$

where $\Delta \boldsymbol{X}_k$ is the vector of all the state variables of the kth WTG; $\boldsymbol{A}_k$, $\boldsymbol{B}_k$ and $\boldsymbol{C}_k$ are the state matrix, control and output matrix of state-space model of the kth WTG respectively. Hence, state-space model of the kth WTG can be denoted as $(\boldsymbol{A}_k, \boldsymbol{B}_k, \boldsymbol{C}_k)$.

From (1) and (2),

$$\begin{aligned}\frac{d}{dt}\Delta \boldsymbol{X}_1 &= \boldsymbol{A}_1\Delta \boldsymbol{X}_1 + (l_{12}+l_{24}+l_{45})\boldsymbol{B}_1\boldsymbol{Z}_C\boldsymbol{C}_1\Delta \boldsymbol{X}_1\\ &\quad + (l_{24}+l_{45})\boldsymbol{B}_1\boldsymbol{Z}_C\boldsymbol{C}_2\Delta \boldsymbol{X}_2 + l_{45}\boldsymbol{B}_1\boldsymbol{Z}_C\boldsymbol{C}_3\Delta \boldsymbol{X}_3\\ \frac{d}{dt}\Delta \boldsymbol{X}_2 &= \boldsymbol{A}_2\Delta \boldsymbol{X}_2 + (l_{24}+l_{45})\boldsymbol{B}_2\boldsymbol{Z}_C\boldsymbol{C}_1\Delta \boldsymbol{X}_1\\ &\quad + (l_{24}+l_{45})\boldsymbol{B}_2\boldsymbol{Z}_C\boldsymbol{C}_2\Delta \boldsymbol{X}_2 + l_{45}\boldsymbol{B}_2\boldsymbol{Z}_C\boldsymbol{C}_3\Delta \boldsymbol{X}_3\\ \frac{d}{dt}\Delta \boldsymbol{X}_3 &= \boldsymbol{A}_3\Delta \boldsymbol{X}_3 + l_{45}\boldsymbol{B}_3\boldsymbol{Z}_C\boldsymbol{C}_1\Delta \boldsymbol{X}_1\\ &\quad + l_{45}\boldsymbol{B}_3\boldsymbol{Z}_C\boldsymbol{C}_2\Delta \boldsymbol{X}_2 + (l_{34}+l_{45})\,\boldsymbol{B}_3\boldsymbol{Z}_C\boldsymbol{C}_3\Delta \boldsymbol{X}_3\end{aligned} \tag{3}$$

Note that the above equations are obtained when the terminal voltage of wind farm is considered to be a constant, because the stability of wind farm as a standalone system is to be examined. The reason is that when the stability of wind farm is examined at the planning stage, it is normally considered that the wind farm is connected to a grid, capacity of which is much greater than that of the wind farm. Hence, the wind farm is planned being connected to an infinite AC busbar with a constant voltage. When the dynamics of external grid need to be considered, equation (3) shall be modified. Subsequently, following derivation should be revised accordingly.

Writing (3) in matrix form, following state-space model of the wind farm is obtained

$$\frac{d}{dt}\Delta \boldsymbol{X}_w = \boldsymbol{A}_w\Delta \boldsymbol{X}_w \tag{4}$$

where $\Delta \boldsymbol{X}_w = [\,\Delta \boldsymbol{X}_1{}^T\ \Delta \boldsymbol{X}_2{}^T\ \Delta \boldsymbol{X}_3{}^T\,]^T$; footnote w refers to the state variable vector and state matrix of the wind farm respectively, unnumbered equation shown at the bottom of this page.

Equation (4) above is referred to as *the full-order model* of the wind farm, where dynamic models of individual WTGs,$(\boldsymbol{A}_k, \boldsymbol{B}_k, \boldsymbol{C}_k), k = 1, 2, 3$, may be different.

$$\boldsymbol{A}_w = \begin{bmatrix} \boldsymbol{A}_1 & \boldsymbol{0} & \boldsymbol{0} \\ \boldsymbol{0} & \mathbf{A}_2 & \boldsymbol{0} \\ \boldsymbol{0} & \boldsymbol{0} & \mathbf{A}_3 \end{bmatrix} + \begin{bmatrix} (l_{12}+l_{24}+l_{45})\mathbf{B}_1\mathbf{Z}_C\mathbf{C}_1 & (l_{24}+l_{45})\mathbf{B}_1\mathbf{Z}_C\mathbf{C}_2 & l_{45}\mathbf{B}_1\mathbf{Z}_C\mathbf{C}_3 \\ (l_{24}+l_{45})\mathbf{B}_2\mathbf{Z}_C\mathbf{C}_1 & (l_{24}+l_{45})\mathbf{B}_2\mathbf{Z}_C\mathbf{C}_2 & l_{45}\mathbf{B}_2\mathbf{Z}_C\mathbf{C}_3 \\ l_{45}\mathbf{B}_3\mathbf{Z}_C\mathbf{C}_1 & l_{45}\mathbf{B}_3\mathbf{Z}_C\mathbf{C}_2 & (l_{34}+l_{45})\,\mathbf{B}_3\mathbf{Z}_C\mathbf{C}_3 \end{bmatrix}$$

B. State-Space Model of the Wind Farm for Planning Grid Connection

At the planning stage, typical parameters of the WTG are usually adopted by the WTGs. It can be considered that the wind speed over the wind farm is not considerably different. Hence, for planning the grid connection of wind farm, it is reasonable to assume that the linearized dynamic models of three WTGs are identical. The state-space models of three WTGs are.

$$(\boldsymbol{A}_k, \boldsymbol{B}_k, \boldsymbol{C}_k) = (\boldsymbol{A}_P, \boldsymbol{B}_P, \boldsymbol{C}_P), k = 1, 2, 3 \tag{5}$$

where footnote p indicates that $(\boldsymbol{A}_P, \boldsymbol{B}_P, \boldsymbol{C}_P)$ refers to the identical state-space model of the WTGs in the wind farm for planning the grid connection. In (5), $\boldsymbol{A}_P \in R^{n\times n}$, $\boldsymbol{B}_P \in R^{n\times 2}$, $\boldsymbol{C}_P \in R^{2\times n}$ with n being the order of dynamic model of the WTG.

From (4) and (5), following state-space model of the wind farm is obtained

$$\frac{d}{dt}\Delta \boldsymbol{X}_w = \boldsymbol{A}\Delta \boldsymbol{X}_w \tag{6}$$

where

$$\boldsymbol{A} = diag[\boldsymbol{A}_p] + \begin{bmatrix} (l_{12}+l_{24}+l_{45})\boldsymbol{I} & (l_{24}+l_{45})\boldsymbol{I} & l_{45}\boldsymbol{I} \\ (l_{24}+l_{45})\boldsymbol{I} & (l_{24}+l_{45})\boldsymbol{I} & l_{45}\boldsymbol{I} \\ l_{45}\boldsymbol{I} & l_{45}\boldsymbol{I} & (l_{34}+l_{45})\boldsymbol{I} \end{bmatrix} \times diag\left[\boldsymbol{B}_P \boldsymbol{Z}_C \boldsymbol{C}_P\right]$$

In (6), $\boldsymbol{A} \in R^{3n\times 3n}$, $\boldsymbol{B}_P\boldsymbol{Z}_C\boldsymbol{C}_P \in R^{n\times n}$; $\boldsymbol{I}$ refers to an $n \times n$ unit matrix; $diag[\boldsymbol{M}]$ refers to a diagonal block matrix with the diagonal matrix to be $\boldsymbol{M}$.

For the convenience of discussion, equation (6) is referred to as the *planning model* of the wind farm. It can be noted from (6) that the state matrix of planning model of the illustrative simple example wind farm $\boldsymbol{A}$ is of a particular structure. The particular structure of $\boldsymbol{A}$ is related with the following structure matrix of the wind farm

$$\boldsymbol{C}_{w3} = \begin{bmatrix} (l_{12}+l_{24}+l_{45}) & (l_{24}+l_{45}) & l_{45} \\ (l_{24}+c_{45}) & (l_{24}+l_{45}) & l_{45} \\ l_{45} & l_{45} & (l_{34}+l_{45}) \end{bmatrix} \in R^{3\times 3} \tag{7}$$

In the next subsection, it is shown that $\boldsymbol{A}$ is similar to a diagonal block matrix which can be established from the computational results of eigenvalues of structure matrix given in (7).

C. Similarity Transformation of State Matrix of Planning Model

Denote $\lambda_k, k = 1, 2, 3$ as the eigenvalues of $\boldsymbol{C}_{\mathrm{w3}}$. There exists a matrix $\boldsymbol{P}_3$ such that

$$\boldsymbol{P}_3\boldsymbol{C}_{\mathrm{w3}}{\boldsymbol{P}_3}^{-1} = diag(\lambda_k) \tag{8}$$

where $diag(\lambda_k)$ denotes a diagonal matrix with the diagonal element to be λ_k.

Let

$$\boldsymbol{P}_3 = \begin{bmatrix} p_{11}\ p_{12}\ p_{13} \\ p_{21}\ p_{22}\ p_{23} \\ p_{31}\ p_{32}\ p_{33} \end{bmatrix}, {\boldsymbol{P}_3}^{-1} = \begin{bmatrix} v_{11}\ v_{12}\ v_{13} \\ v_{21}\ v_{22}\ v_{23} \\ v_{31}\ v_{32}\ v_{33} \end{bmatrix} \tag{9}$$

It can have

$$\boldsymbol{P}_3{\boldsymbol{P}_3}^{-1} = \begin{bmatrix} p_{11}\ p_{12}\ p_{13} \\ p_{21}\ p_{22}\ p_{23} \\ p_{31}\ p_{32}\ p_{33} \end{bmatrix} \begin{bmatrix} v_{11}\ v_{12}\ v_{13} \\ v_{21}\ v_{22}\ v_{23} \\ v_{31}\ v_{32}\ v_{33} \end{bmatrix} = \begin{bmatrix} 1\ 0\ 0 \\ 0\ 1\ 0 \\ 0\ 0\ 1 \end{bmatrix} = \boldsymbol{I}_3 \in R^{3\times 3} \tag{10}$$

Define following similarity transformation matrix

$$\boldsymbol{P}_{3n} = \begin{bmatrix} p_{11}\boldsymbol{I}\ p_{12}\boldsymbol{I}\ p_{13}\boldsymbol{I} \\ p_{21}\boldsymbol{I}\ p_{22}\boldsymbol{I}\ p_{23}\boldsymbol{I} \\ p_{31}\boldsymbol{I}\ p_{32}\boldsymbol{I}\ p_{33}\boldsymbol{I} \end{bmatrix}, {\boldsymbol{P}_{3n}}^{-1} = \begin{bmatrix} v_{11}\boldsymbol{I}\ v_{12}\boldsymbol{I}\ v_{13}\boldsymbol{I} \\ v_{21}\boldsymbol{I}\ v_{22}\boldsymbol{I}\ v_{23}\boldsymbol{I} \\ v_{31}\boldsymbol{I}\ v_{32}\boldsymbol{I}\ v_{33}\boldsymbol{I} \end{bmatrix} \tag{11}$$

where $\boldsymbol{P}_{3n} \in R^{3n\times 3n}$, ${\boldsymbol{P}_{3n}}^{-1} \in R^{3n\times 3n}$. It can easily be proved that

$$\begin{aligned} \boldsymbol{P}_{3n}{\boldsymbol{P}_{3n}}^{-1} &= diag\left[\boldsymbol{I}\right] \in R^{3n\times 3n} \\ \boldsymbol{P}_{3n}\boldsymbol{C}_{3n}{\boldsymbol{P}_{3n}}^{-1} &= diag\left[\lambda_k\boldsymbol{I}\right] \in R^{3n\times 3n} \end{aligned} \tag{12}$$

where

$$\boldsymbol{C}_{3n} = \begin{bmatrix} (l_{12}+l_{24}+l_{45})\boldsymbol{I} & (l_{24}+l_{45})\boldsymbol{I} & l_{45}\boldsymbol{I} \\ (l_{24}+l_{45})\boldsymbol{I} & (l_{24}+l_{45})\boldsymbol{I} & l_{45}\boldsymbol{I} \\ l_{45}\boldsymbol{I} & l_{45}\boldsymbol{I} & (l_{34}+l_{45})\boldsymbol{I} \end{bmatrix} \in R^{3n\times 3n}$$

From (10), (11) and (12),

$$\begin{aligned} &\begin{bmatrix} p_{11}\boldsymbol{I}\ p_{12}\boldsymbol{I}\ p_{13}\boldsymbol{I} \\ p_{21}\boldsymbol{I}\ p_{22}\boldsymbol{I}\ p_{23}\boldsymbol{I} \\ p_{31}\boldsymbol{I}\ p_{32}\boldsymbol{I}\ p_{33}\boldsymbol{I} \end{bmatrix} diag\left[\boldsymbol{A}_p\right] \begin{bmatrix} v_{11}\boldsymbol{I}\ v_{12}\boldsymbol{I}\ v_{13}\boldsymbol{I} \\ v_{21}\boldsymbol{I}\ v_{22}\boldsymbol{I}\ v_{23}\boldsymbol{I} \\ v_{31}\boldsymbol{I}\ v_{32}\boldsymbol{I}\ v_{33}\boldsymbol{I} \end{bmatrix} \\ &= diag\left[\boldsymbol{A}_p\right] \begin{bmatrix} p_{11}\boldsymbol{I}\ p_{12}\boldsymbol{I}\ p_{13}\boldsymbol{I} \\ p_{21}\boldsymbol{I}\ p_{22}\boldsymbol{I}\ p_{23}\boldsymbol{I} \\ p_{31}\boldsymbol{I}\ p_{32}\boldsymbol{I}\ p_{33}\boldsymbol{I} \end{bmatrix} \begin{bmatrix} v_{11}\boldsymbol{I}\ v_{12}\boldsymbol{I}\ v_{13}\boldsymbol{I} \\ v_{21}\boldsymbol{I}\ v_{22}\boldsymbol{I}\ v_{23}\boldsymbol{I} \\ v_{31}\boldsymbol{I}\ v_{32}\boldsymbol{I}\ v_{33}\boldsymbol{I} \end{bmatrix} \\ &= \begin{bmatrix} \boldsymbol{A}_p & \boldsymbol{0} & \boldsymbol{0} \\ \boldsymbol{0} & \boldsymbol{A}_p & \boldsymbol{0} \\ \boldsymbol{0} & \boldsymbol{0} & \boldsymbol{A}_p \end{bmatrix} \begin{bmatrix} \boldsymbol{I}\ \boldsymbol{0}\ \boldsymbol{0} \\ \boldsymbol{0}\ \boldsymbol{I}\ \boldsymbol{0} \\ \boldsymbol{0}\ \boldsymbol{0}\ \boldsymbol{I} \end{bmatrix} = diag\left[\boldsymbol{A}_p\right] \end{aligned} \tag{13}$$

Similarly, from (7),

$$\begin{aligned} &\begin{bmatrix} p_{11}\boldsymbol{I}\ p_{12}\boldsymbol{I}\ p_{13}\boldsymbol{I} \\ p_{21}\boldsymbol{I}\ p_{22}\boldsymbol{I}\ p_{23}\boldsymbol{I} \\ p_{31}\boldsymbol{I}\ p_{32}\boldsymbol{I}\ p_{33}\boldsymbol{I} \end{bmatrix} \begin{bmatrix} (l_{12}+l_{24}+l_{45})\boldsymbol{I} & (l_{24}+l_{45})\boldsymbol{I} & l_{45}\boldsymbol{I} \\ (l_{24}+l_{45})\boldsymbol{I} & (l_{24}+l_{45})\boldsymbol{I} & l_{45}\boldsymbol{I} \\ l_{45}\boldsymbol{I} & l_{45}\boldsymbol{I} & (l_{34}+l_{45})\boldsymbol{I} \end{bmatrix} \\ &\times diag\left[\boldsymbol{B}_P\boldsymbol{Z}_C\boldsymbol{C}_P\right] \begin{bmatrix} v_{11}\boldsymbol{I}\ v_{12}\boldsymbol{I}\ v_{13}\boldsymbol{I} \\ v_{21}\boldsymbol{I}\ v_{22}\boldsymbol{I}\ v_{23}\boldsymbol{I} \\ v_{31}\boldsymbol{I}\ v_{32}\boldsymbol{I}\ v_{33}\boldsymbol{I} \end{bmatrix} = \begin{bmatrix} p_{11}\boldsymbol{I}\ p_{12}\boldsymbol{I}\ p_{13}\boldsymbol{I} \\ p_{21}\boldsymbol{I}\ p_{22}\boldsymbol{I}\ p_{23}\boldsymbol{I} \\ p_{31}\boldsymbol{I}\ p_{32}\boldsymbol{I}\ p_{33}\boldsymbol{I} \end{bmatrix} \\ &\times \begin{bmatrix} (l_{12}+l_{24}+l_{45})\boldsymbol{I} & (l_{24}+l_{45})\boldsymbol{I} & l_{45}\boldsymbol{I} \\ (l_{24}+l_{45})\boldsymbol{I} & (l_{24}+l_{45})\boldsymbol{I} & l_{45}\boldsymbol{I} \\ l_{45}\boldsymbol{I} & l_{45}\boldsymbol{I} & (l_{34}+l_{45})\boldsymbol{I} \end{bmatrix} \\ &\times \begin{bmatrix} v_{11}\boldsymbol{I}\ v_{12}\boldsymbol{I}\ v_{13}\boldsymbol{I} \\ v_{21}\boldsymbol{I}\ v_{22}\boldsymbol{I}\ v_{23}\boldsymbol{I} \\ v_{31}\boldsymbol{I}\ v_{32}\boldsymbol{I}\ v_{33}\boldsymbol{I} \end{bmatrix} diag\left[\boldsymbol{B}_P\boldsymbol{Z}_C\boldsymbol{C}_P\right] \\ &= diag\left[\lambda_k\boldsymbol{I}\right] diag\left[\boldsymbol{B}_P\boldsymbol{Z}_1\boldsymbol{C}_P\right] = diag\left[\lambda_k\boldsymbol{B}_P\boldsymbol{Z}_C\boldsymbol{C}_P\right] \end{aligned} \tag{14}$$

From (6), (13) and (14),

$$\boldsymbol{P}_{3n}\boldsymbol{A}{\boldsymbol{P}_{3n}}^{-1} = diag\left[\boldsymbol{A}_p + \lambda_k\boldsymbol{B}_P\boldsymbol{Z}_C\boldsymbol{C}_P\right] \tag{15}$$

Hence, the state matrix of planning model of the wind farm, $\boldsymbol{A}$, is similar to $diag[\boldsymbol{A}_p + \lambda_k\boldsymbol{B}_P\boldsymbol{Z}_C\boldsymbol{C}_P]$. Modal computation

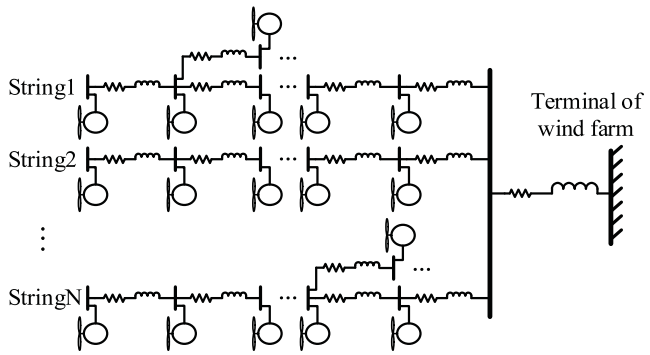

Fig. 2. Configuration of a large-scale wind farm with *m* WTGs.

of the wind farm can be conducted by calculating the eigenvalues of diagonal element matrices, $\boldsymbol{A}_p + \lambda_k \boldsymbol{B}_P \boldsymbol{Z}_C \boldsymbol{C}_P, k = 1, 2, 3$. Dimension of full-order state matrix, $\boldsymbol{A}$, is $3n$. Dimension of diagonal matrices, $\boldsymbol{A}_p + \lambda_k \boldsymbol{B}_P \boldsymbol{Z}_C \boldsymbol{C}_P, k = 1, 2, 3$, is n. Dimension of structure matrix $\boldsymbol{C}_{w3}$ is 3. Hence, modal computation of $\boldsymbol{A}$ by calculating eigenvalues of $\boldsymbol{C}_{w3}$ and $\boldsymbol{A}_p + \lambda_k \boldsymbol{B}_P \boldsymbol{Z}_C \boldsymbol{C}_P, k = 1, 2, 3$ is reduced-order.

Extension of the derivation presented above to a large-scale wind farm with m WTGs is introduced in the next section. Thus, the order reduction is from nm to n and m, which could be significant when there are large number of WTGs in the wind farm.

III. Method of Reduced-Order Modal Computation

Configuration of a general large-scale wind farm is shown by Fig. 2. There are m WTGs in the wind farm arranged in *N* strings. Radial topology of the wind farm's network is due to the fact that the wind farm is mainly for the power collection from the WTGs. To plan the grid connection of the wind farm, state-space model of the individual WTGs, $(\boldsymbol{A}_P, \boldsymbol{B}_P, \boldsymbol{C}_P)$, can be obtained with the typical operating condition and parameters of the WTGs being used.

Taking the derivation similar to that from (1) to (6), following planning model of the wind farm can be obtained

$$\frac{d}{dt}\Delta \boldsymbol{X}_w = \boldsymbol{A}\Delta \boldsymbol{X}_w \tag{16}$$

where

$$\Delta \boldsymbol{X}_w = \left[\, \Delta \boldsymbol{X}_1{}^T \; \Delta \boldsymbol{X}_2{}^T \; \cdots \; \Delta \boldsymbol{X}_m{}^T \,\right]^T$$

$$\boldsymbol{A} = \operatorname{diag}\left[\boldsymbol{A}_p\right] + \begin{bmatrix} c_{11}\boldsymbol{I} & c_{12}\boldsymbol{I} & \cdots & c_{1m}\boldsymbol{I} \\ c_{21}\boldsymbol{I} & c_{22}\boldsymbol{I} & \cdots & c_{2m}\boldsymbol{I} \\ \vdots & \vdots & \ddots & \vdots \\ c_{m1}\boldsymbol{I} & c_{m2}\boldsymbol{I} & \cdots & c_{mm}\boldsymbol{I} \end{bmatrix} diag\left[\boldsymbol{B}_p \boldsymbol{Z}_C \boldsymbol{C}_p\right]$$

$\boldsymbol{A} \in R^{mn \times mn}$, $\boldsymbol{B}_P \boldsymbol{Z}_C \boldsymbol{C}_P \in R^{n \times n}$ and $\boldsymbol{I}$ is a $n \times n$ unit matrix (*n* is the order of dynamic model of individual WTGs).

In (16), $c_{ij}, i, j = 1, 2, \ldots, m$ are the elements of following structure matrix of the wind farm

$$\boldsymbol{C}_{wm} = [c_{ij}] \in R^{m \times m} \tag{17}$$

Rules forming the structure matrix are:

1) Diagonal element, $c_{ii}, i = 1, 2, \ldots, m$, is the total length of the cable from the ith WTG to the terminal of the wind farm;
2) Non-diagonal element, $c_{ij}, i, j = 1, 2, \ldots, m$ is the length of a segment of cable. The segment of cable is the common part of the cables connecting the ith and jth WTG to the terminal of wind farm.

Denote $\lambda_k, k = 1, 2, \ldots, m$ as the eigenvalues of $\boldsymbol{C}_{wm}$. It can be proved that the full-order state matrix, $\boldsymbol{A}$ in (14), is similar to the following diagonal block matrix $diag[\boldsymbol{A}_p + \lambda_k \boldsymbol{B}_P \boldsymbol{Z}_C \boldsymbol{C}_P]$, i.e., the state matrix of planning model is similar to a matrix $\boldsymbol{A}_E$.

The proof is similar to that from (6) to (15) and presented in Appendix A. For the convenience of discussion, state-space model of the wind farm with the state matrix being given by (18) shown at the bottom of this page, is referred to as the *similar model* of the wind farm.

It can be noted that the order of similar model of the wind farm is still nm, which is as same as that of full-order model and planning model of the wind farm. Hence, the derivation above just proves that the wind farm can be equivalently represented by *m* dynamic independent subsystems, rather than produces a reduced-order model of the wind farm. State matrices of each of the subsystems are $\boldsymbol{A}_p + \lambda_k \boldsymbol{B}_P \boldsymbol{Z}_C \boldsymbol{C}_P, k = 1, 2, \ldots, m$. The subsystems fully keep the information about the dynamics of individual WTGs as $(\boldsymbol{A}_P, \boldsymbol{B}_P, \boldsymbol{C}_P)$ and the topology of the wind farm as the eigenvalues of structure matrix, $\lambda_k, k = 1, 2, \ldots, m$. Hence, the equivalence established above can stand when the operating conditions of WTGs and topology of wind farm vary.

From (18), a method of reduced-order modal computation can be proposed as follows.

1) Establish the state-space model of a single WTG in the wind farm, $(\boldsymbol{A}_P, \boldsymbol{B}_P, \boldsymbol{C}_P)$, by using the typical parameters and operating conditions of the WTG.
2) Establish the structure matrix of the wind farm, $\boldsymbol{C}_{wm} = [c_{ij}] \in R^{m \times m}$, according to the rules given above.
3) Calculate the eigenvalues of $\boldsymbol{C}_{\mathrm{wm}} = [c_{ij}] \in R^{m \times m}$ to be $\lambda_k, k = 1, 2, \ldots, m$.
4) Calculate the eigenvalues of following matrices to assess the small-signal stability of the wind farm

$$(\boldsymbol{A}_p + \lambda_k \boldsymbol{B}_P \boldsymbol{Z}_C \boldsymbol{C}_P) \in R^{n \times n}, k = 1, 2, \ldots, m \tag{19}$$

Dimension of state matrix of the wind farm is mn. The dimensions of matrices involved in the method of modal computation

$$\boldsymbol{A}_E = \begin{bmatrix} \boldsymbol{A}_p + \lambda_1 \boldsymbol{B}_p \boldsymbol{Z}_C \boldsymbol{C}_p & \mathbf{0} & \cdots & \mathbf{0} \\ \mathbf{0} & \mathbf{A}_p + \lambda_2 \mathbf{B}_p \mathbf{Z}_C \mathbf{C}_p & \cdots & \mathbf{0} \\ \vdots & \vdots & \ddots & \vdots \\ \mathbf{0} & \mathbf{0} & \cdots & \mathbf{A}_p + \lambda_m \mathbf{B}_p \mathbf{Z}_C \mathbf{C}_p \end{bmatrix} \tag{18}$$

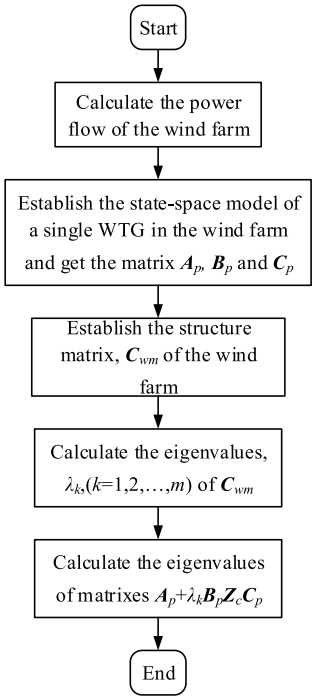

Fig. 3. Flowchart of processes of the reduced-order method of modal computation.

proposed above are n and m. Hence, it is reduced-order method of modal computation.

Fig. 3 shows the flowchart of process of reduced-order model computation proposed.

IV. An Illustrative Simple Example Wind Farm

For the tutorial purpose, an illustrative simple example wind farm is used to validate and demonstrate the reduced-order method of modal computation proposed in the previous section. Configuration of the example wind farm is as same as that displayed in Fig. 1. The WTGs in Fig. 1 are replaced by the PMSGs. Two cases are studied when simplified and detailed model of PMSG are adopted respectively.

A. Study Case A: Simplified Model of PMSG is Used

Each of the PMSGs in the simple example wind farm is modelled as a constant voltage source at the terminal of its grid side converter (GSC), $V_{cx0} + jV_{cy0}$. Thus, linearized voltage equation of the line connecting the *k*th PMSG to node *k* in the wind farm can be obtained to be

$$\begin{aligned} \frac{\mathrm{d}}{dt}\Delta I_{kx} &= -\frac{\omega_0}{X_k}\Delta V_{kx} + \omega_0 \Delta I_{ky} \\ \frac{\mathrm{d}}{dt}\Delta I_{ky} &= -\frac{\omega_0}{X_k}\Delta V_{ky} - \omega_0 \Delta I_{kx} \end{aligned}, k = 1,2,3 \tag{20}$$

where $\omega_0 = 120\pi$ and X_k is the equivalent reactance of the low/middle voltage transformer plus the reactance of the output filter of the *k*th PMSG.

Expressing (20) in the matrix form of (2), it can have $(n = 2)$

$$\begin{aligned} \Delta \boldsymbol{X}_k &= \left[\Delta I_{kx}\ \Delta I_{ky}\right]^T, k = 1,2,3 \\ \boldsymbol{A}_p &= \begin{bmatrix} 0 & \omega_0 \\ -\omega_0 & 0 \end{bmatrix} = \begin{bmatrix} 0 & 376.99 \\ -376.99 & 0 \end{bmatrix} \\ \boldsymbol{B}_p &= \begin{bmatrix} -\frac{\omega_0}{X_{\mathrm{pf}}} & 0 \\ 0 & -\frac{\omega_0}{X_{\mathrm{pf}}} \end{bmatrix} = \begin{bmatrix} -18850 & 0 \\ 0 & -18850 \end{bmatrix} \\ \boldsymbol{C}_p &= \begin{bmatrix} 1 & 0 \\ 0 & 1 \end{bmatrix} \end{aligned} \tag{21}$$

The length of cable in each section of the illustrative simple example wind farm is $l_{12} = 0.7$ km, $l_{24} = 0.5$ km, $l_{34} = 0.8$ km and $l_{45} = 1.5$ km respectively. The structure matrix of the wind farm, $\boldsymbol{C}_{w3}$ in (7), is formed as follows.

1) Cable length from node 1 to the terminal of wind farm is $l_{12} + l_{24} + l_{45}$. Hence, $c_{11} = l_{12} + l_{24} + l_{45} = 2.7$. Similarly, $c_{22} = l_{24} + l_{45} = 2.0$ and $c_{33} = l_{34} + l_{45} = 2.3$.
2) The length of the segment of cable commonly used by the 1st and 2nd PMSG to connect the 1st and 2nd PMSG to the terminal of the wind farm is $c_{12} = c_{21} = l_{24} + l_{45} = 2.0$. Similarly, $c_{13} = c_{31} = l_{45} = 1.5$, which is the length of segment of cable commonly used by the 1st and 3rd PMSG. $c_{23} = c_{32} = l_{45} = 1.5$, which is the length of segment of cable commonly used by the 2nd and 3rd PMSG.

Thus, structure matrix of the wind farm is $\boldsymbol{C}_{w3}$ in (5), i.e.,

$$\boldsymbol{C}_{w3} = \begin{bmatrix} 2.7 & 2 & 1.5 \\ 2 & 2 & 1.5 \\ 1.5 & 1.5 & 2.3 \end{bmatrix} \tag{22}$$

Eigenvalues of $\boldsymbol{C}_{w3}$ was calculated to be

$$\lambda_1 = 0.2833,\ \lambda_2 = 1.0193,\ \lambda_3 = 5.6974 \tag{23}$$

Impedance of the cable/per km. is $Z_C = 0.0175 + j0.0367$ [19]. Hence, $\boldsymbol{Z}_C = \left[\begin{smallmatrix} R_C & -X_C \\ X_C & R_C \end{smallmatrix}\right] = \left[\begin{smallmatrix} 0.0175 & -0.0367 \\ 0.0367 & 0.0175 \end{smallmatrix}\right]$. From (21),

$$\boldsymbol{B}_P \boldsymbol{Z}_C \boldsymbol{C}_P = \begin{bmatrix} -329.87 & 683.67 \\ -683.67 & -329.87 \end{bmatrix} \tag{24}$$

Thus, according to (18), following three 2×2 matrices are derived

$$\begin{aligned} \boldsymbol{A}_p + 0.2833\boldsymbol{B}_P \boldsymbol{Z}_C \boldsymbol{C}_P &= \begin{bmatrix} -93.44 & 570.65 \\ -570.65 & -93.44 \end{bmatrix} \\ \boldsymbol{A}_p + 1.0193\boldsymbol{B}_P \boldsymbol{Z}_C \boldsymbol{C}_P &= \begin{bmatrix} -336.24 & 1073.86 \\ -1073.86 & -336.24 \end{bmatrix} \\ \boldsymbol{A}_p + 5.6974\boldsymbol{B}_P \boldsymbol{Z}_C \boldsymbol{C}_P &= \begin{bmatrix} -1879.40 & 4272.18 \\ -4272.18 & -1879.40 \end{bmatrix} \end{aligned} \tag{25}$$

Eigenvalues of matrices in (25) are calculated to be

$$\begin{aligned} &-1879.4 \pm j4272.2, -336.24 \pm j1073.9, \\ &-93.437 \pm j570.65 \end{aligned} \tag{26}$$

Those above are the results of reduced-order modal computation.

For confirmation, state matrix of the full-order model of wind farm, $\boldsymbol{A}_w$ given in (4), is derived to be

$$\boldsymbol{A}_w = \begin{bmatrix} -890.64 & 2222.9 & -659.73 & 1367.3 & -494.8 & 1025.5 \\ -2222.9 & -890.64 & -1367.3 & -659.73 & -1025.5 & -494.8 \\ -659.73 & 1367.3 & -659.73 & 1744.3 & -494.8 & 1025.5 \\ -1367.3 & -659.73 & -1744.3 & -659.73 & -1025.5 & -494.8 \\ -494.8 & 1025.5 & -494.8 & 1025.5 & -758.69 & 1949.4 \\ -1025.5 & -494.8 & -1025.5 & -494.8 & -1949.4 & -758.69 \end{bmatrix}$$

Eigenvalues of $\boldsymbol{A}_w$ are computed and are exactly as same as those obtained above in (26) by using the reduced-order method of modal computation.

From (21), it can be noted that the state-space model of the PMSG is irrelevant with the operating condition when the PMSG is modelled as the constant voltage source. Thus, the state-space models of three PMSGs, $(\boldsymbol{A}_P, \boldsymbol{B}_P, \boldsymbol{C}_P)$ given in (21), are identical. Subsequently, state matrix of full-order model is as same as that of the planning model of the wind farm, which is equivalent to the similar model. This is why the results of modal computation by using the similar model are as same as those by using the full-order model.

B. Study Case B: Detailed Model of PMSG Is Used

The operating conditions of the PMSGs are normally different in the wind farm. Hence, the state-space models of individual PMSGs should be slightly different from each other even if it is assumed that all the PMSGs operate at the same wind speed and their parameters are of the same values. In this subsection, this particular aspect is evaluated by using the detailed model of PMSG.

In the simple example wind farm shown by Fig. 1 with three PMSGs, the 15th-order dynamic model and parameters used in [20] are adopted $(n = 15)$. Active power output at steady state from each of three PMSGs is 2.5 p.u. Hence, all three PMSGs operate at the same wind speed. In addition, they all operate with unit power factor. Based on the computational results of power flow in the wind farm, linearized state-space models of the PMSGs displayed in (2) are established. It is found that $(\boldsymbol{A}_k, \boldsymbol{B}_k, \boldsymbol{C}_k), k = 1, 2, 3$ are different $(\boldsymbol{A}_k \in R^{15\times 15}, \boldsymbol{B}_k \in R^{15\times 2}$ and $\boldsymbol{C}_k \in R^{2\times 15})$. Following tests are conducted to evaluate the proposed reduced-order method of modal computation.

First, $(\boldsymbol{A}_1, \boldsymbol{B}_1, \boldsymbol{C}_1)$ is used to represent all three PMSGs. This is to assume that $(\boldsymbol{A}_P, \boldsymbol{B}_P, \boldsymbol{C}_P) = (\boldsymbol{A}_1, \boldsymbol{B}_1, \boldsymbol{C}_1)$. Under this assumption, Reduced-order modal computation is conducted and the computational results are presented in the first column of Table I. Second, take $(\boldsymbol{A}_P, \boldsymbol{B}_P, \boldsymbol{C}_P) = (\boldsymbol{A}_2, \boldsymbol{B}_2, \boldsymbol{C}_2)$ and $(\boldsymbol{A}_P, \boldsymbol{B}_P, \boldsymbol{C}_P) = (\boldsymbol{A}_3, \boldsymbol{B}_3, \boldsymbol{C}_3)$ respectively by using the 2nd and 3rd PMSG as the representative of three PMSGs respectively. Results of reduced-order modal computation are obtained and presented in the second and third column of Table I. Note that in Table I, only oscillation modes of simple example wind farm are listed.

For comparison, oscillation modes of simple example wind farm are computed by using its full-order model. Computational results are displayed in the fourth column of Table I. Denote λ_S and λ_F as the oscillation mode computed by using the similar model and full-order model of wind farm respectively. Computational errors are defined as

$$error = \frac{100\,|\lambda_S - \lambda_F|}{|\lambda_F|}\% \tag{27}$$

In the last row of Table I, on-average computational errors defined above are presented.

Results of modal computation displayed in Table I confirm that the reduced-order method of modal computation is effective to assess the small-signal stability of the simple example wind farm.

TABLE I
RESULTS OF REDUCED-ORDER MODAL COMPUTATION

Similar model and $(\boldsymbol{A}_1, \boldsymbol{B}_1, \boldsymbol{C}_1)$ used	Similar model and $(\boldsymbol{A}_2, \boldsymbol{B}_2, \boldsymbol{C}_2)$ used	Similar model and $(\boldsymbol{A}_3, \boldsymbol{B}_3, \boldsymbol{C}_3)$ used	Full-order model used
-65.92+j574.92	-65.46+j571.18	-65.39+j570.59	-65.58+j572.49
-77.23+j558.93	-76.27+j555.53	-76.11+j554.99	-76.66+j556.89
-76.33+j555.16	-75.33+j551.65	-75.17+j551.09	-75.42+j552.05
-54.11+j483.99	-53.46+j478.03	-53.34+j477.09	-53.67+j480.15
-49.81+j512.61	-49.81+j507.29	-49.81+j506.45	-49.78+j507.90
-49.71+j515.18	-49.71+j509.86	-49.71+j509.02	-49.80+j511.80
-5.14+j130.02	-5.08+j128.37	-5.07+j128.11	-5.09+j128.89
-5.58+j137.70	-5.45+j136.10	-5.43+j135.84	-5.51+j136.84
-5.48+j136.78	-5.35+j135.14	-5.33+j134.88	-5.36+j135.25
-3.63+j85.16	-3.53+j84.26	-3.51+j84.10	-3.57+j84.65
-4.11+j87.64	-4.12+j87.55	-4.12+j87.53	-4.12+j87.56
-4.14+j88.13	-4.16+j88.06	-4.16+j88.05	-4.15+j88.05
0.6%	0.25%	0.39%	

V. AN EXAMPLE LARGE-SCALE WIND FARM

A. Reduced-Order Model Computation

An example large-scale wind farm with 200 PMSGs is used to evaluate and demonstrate the reduced-order method of modal computation in this section. Configuration and cable parameters of the wind farm are given in Appendix B. To plan the grid connection of the wind farm, typical parameters and the 15th-order model of the PMSG used in [20] are adopted. Dimension of structure matrix of the wind farm is 200, which is the highest dimension of matrices when the proposed method of reduced-order modal computation is used to assess the small-signal stability of the wind farm. For confirmation, state matrix of full-order model of the wind farm, $\boldsymbol{A}_w$, is also derived and used to calculate the oscillation modes. Dimension of $\boldsymbol{A}_w$ is 3000. Clearly, the reduction for the modal computation by the proposed method is significant.

When the standard function to calculate the eigenvalues of a matrix in the MATLAB is used, a laboratory PC (Intel(R)

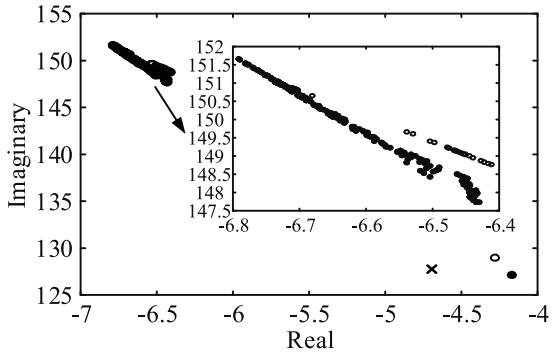

Fig. 4. Oscillation modes dominated by the PLLs of the PMSGs in the example large-scale wind farm.

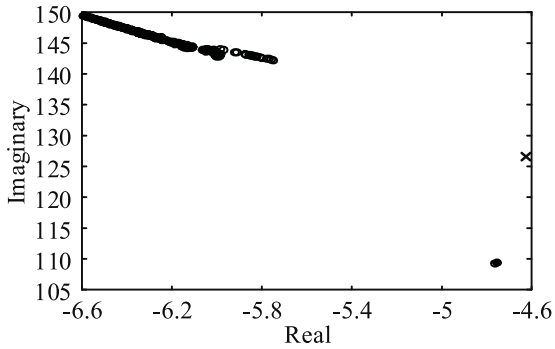

Fig. 6. Oscillation modes dominated by the PLLs of the PMSGs in the example large-scale wind farm when the PMSGs were distributed in an increased area.

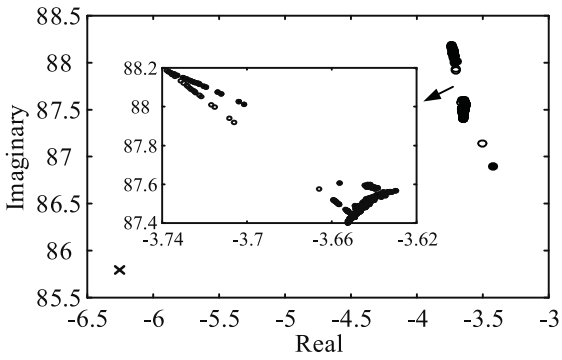

Fig. 5. Oscillation modes dominated by DC voltage control loops of the GSCs of the PMSGs in the example large-scale wind farm.

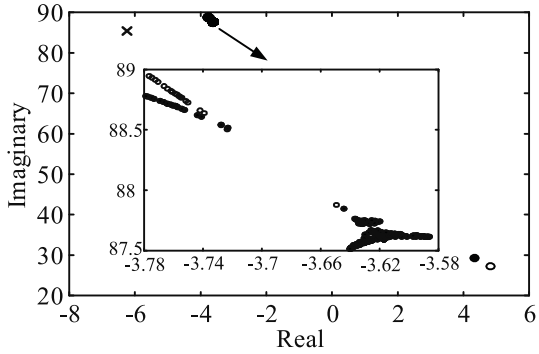

Fig. 7. Oscillation modes dominated by DC voltage control loops of the GSCs of the PMSGs in the example large-scale wind farm when the PMSGs were distributed in an increased area.

Core(TM) i5-4570 CPU @ 3.20GHz) takes about 0.0949 seconds to produce the results of modal computation by using the proposed method. However, it takes about 24.8227 seconds to directly calculate the eigenvalues of a 3000-dimensional matrix. In addition, storage needed for the direct computation of eigenvalues of 3000-dimensional matrix in one computation is $3000 \times 3000 = 9 \times 10^6$ (floating-point number). That needed by the proposed method is $200 \times 15 \times 15 = 4.5 \times 10^4$ (floating-point number). With improved programming, only $\boldsymbol{A}_p$, $\boldsymbol{A}_n$, $\boldsymbol{A}_p + \lambda_i \boldsymbol{A}_n$ and $\lambda_k, k = 1, 2, \ldots, 200$ need to be stored. Hence, the storage needed is only about $200 + 15 \times 15 \times 3 = 875$ (floating- point number). The proposed method of reduced-order modal computation reduces both the computational time and storage considerably. This feature is very attractive when large-scale wind farms are planned for the grid-connection and numerous scenarios need to be considered. Hence, further investigation on the improvement of computational efficiency of the proposed method in programming is needed.

It has been found that the oscillation modes associated with the PLLs and DC voltage control outer loops of the GSCs of the PMSGs are usually prone to poor or even negative damping. Hence, it is essentially important to find those two types of oscillation modes in assessing the small-signal stability of the wind farm. Fig. 4 and Fig. 5 show the computational results of the oscillation modes of the example large-scale wind farm on the complex plane by using the reduced-order method and state matrix of full-order model of the wind farm. In Fig. 4 and Fig. 5, hollow circles are computed by using the reduced-order method and the filled circles are the true positions of oscillation modes computed by using the full-order model of the wind farm. It can be seen that the proposed method of reduced-order modal computation is effective to estimate the oscillation modes of the large-scale wind farm, though there are small differences between the results of reduce-order and full-order modal computation. The difference is due to the fact that state-space models of PMSGs in the wind farm are not identical. Consequently, full-order model and planning model of the wind farm are slightly different.

To gain a more efficient capture of wind power, an alternative plan for the example large-scale wind farm is to distribute 200 PMSGs in an increased geographical area by 1.6 times. The alternative plan is examined to consider the impact of increased geographical area of PMSGs' distribution on the small-signal stability of the wind farm as follows.

With the increase of geographical area of the wind farm by 1.6 times, it is assumed that the length of every segment of cable is increased by 1.6 times. Then, the proposed method of reduced-order modal computation is used to estimate the small-signal stability of the wind farm. In Fig. 6 and 7, the positions of oscillation modes associated with the PLLs and DC voltage control outer loops of the GSCs on the complex plane obtained by using the proposed method of reduced-order modal computation

TABLE II
THREE MOST LIGHTLY DAMPED OSCILLATION MODES AND COMPUTATIONAL ERRORS

Fig. 4 and Fig. 5			Fig. 6 and Fig. 7		
Similar model used	full-order model used	Error	Similar model used	full-order model used	Error
-4.16 +j127.04	-4.17 +j127.11	0.06 %	-4.76 +j109.33	-4.75 +j109.38	0.05 %
-6.19 +j146.08	-6.43 +j147.73	1.13 %	-5.55 +j139.63	-5.99+ j143.20	2.51 %
-6.20 +146.09	-6.43 +j147.98	1.28 %	-5.58 +j139.70	-5.99 +j143.12	2.4%
-3.42 +j86.81	-3.42 +j86.89	0.09 %	4.83 +j27.33	4.32 +j29.34	6.98 %
-3.63 +j87.56	-3.62 +j87.57	0	-3.58 +j87.61	-3.59 +j87.62	0
-3.63 +j87.56	-3.63 +j87.57	0	-3.58 +j87.62	-3.59 +j87.62	0

are indicated by hollow circles. For comparison, the oscillation modes are computed by using the full-order model of the wind farm. The computational results are indicated by filled circles in Fig. 6 and 7.

Fig. 6 and 7 demonstrate that the proposed method of reduced-order modal computation is effective to estimate the small-signal stability of the wind farm. The example large-scale wind farm becomes unstable when 200 PMSGs are distributed in the increased geographical area.

Three most lightly damped oscillation modes are selected from those displayed in Fig. 4, 5, 6 and 7 respectively. Those selected oscillation modes calculated by using the similar model (i.e., the reduced-order modal computation) are listed in Table II. Computational errors as compared with the computational results from the full-order model of wind farm are also presented in Table II. It can be seen that computational errors are very small and completely acceptable for the purpose of stability assessment in planning the grid connection of the wind farm.

B. Comparison With the CMV Method

According to the wind farm modelling guide recommended by the International Electrotechnical Commission (IEC) and Western Electricity Coordinating Council (WECC), a wind farm can be modelled as an aggregated WTG with the increased capacity. Parameters of the WTG with the increased capacity are calculated by the capacity-weighted mean value (CMV) method [21]. Wind farm network is represented by an aggregated impedance, which is calculated based on the equivalent amount of power loss [22]. The CMV method has been widely used to obtain the reduced-order model of the wind farm, particularly for planning the grid connection of wind farm [10]–[12], [21], [22].

For the large-scale example with 200 PMSG, a reduced-order model is derived by using the CMV method as an aggregated PMSG with the increased capacity. The oscillation modes associated with the PLL and DC voltage control outer loop of the GSC of the aggregated PMSG are calculated. They are indicated by crosses in Fig. 4, 5, 6 and 7. It can be seen that the computational results of proposed method of reduced-order modal computation are much closer to the actual results than those obtained by using the CMV method. Errors of CMV method are obviously bigger. Note that when the CMV method is used, the aggregated PMSG is of only one oscillation mode associated with either the PLL or the DC voltage control outer loop of the GSC.

TABLE III
OSCILLATION MODE OF THE WIND FARM CALCULATED BY USING THE CMV METHOD BEFORE AND AFTER THE GEOGRAPHICAL AREA IS INCREASED BY 1.6 TIMES

Before	After
-4.69+j127.79	-4.63+j126.63
-6.25+j85.79	-6.23+j85.41

In addition, when the CMV method is used, instability risk associated with the planned increase of geographical area of wind farm by 1.6 times cannot be identified. This is because in Fig. 6 and Fig. 7, the CMV method indicates that the oscillation modes of wind farm are still of sufficient damping, though the wind farm already becomes unstable. From further comparison between Fig. 4 and 6 as well as between Fig. 5 and 7, it can be found that in fact before and after the geographical area of wind farm increases, the oscillation modes calculated by using the CMV method change only slightly as displayed in Table III. This confirms that the variation of topology of wind farm cannot be reflected in the CMV method. The variation is well captured by the proposed method of reduced-order modal computation.

C. Selection of Representative PMSG

In planning the grid connection of a wind farm, the WTGs in different areas in the wind farm may take different typical parameters due to various technical considerations, such as the wind conditions. Hence, dynamic models of the WTGs in the whole wind farm may not be identical even at the planning stage. This subsection demonstrates how the proposed method of reduced-order modal computation can be applied in this particular case to examine the stability of the example large-scale wind farm. The key step in the application is the selection of models of PMSGs to represent all the PMSGs in the wind farm.

It is assumed that 200 PMSGs are planned to be located in three different areas in the example large-scale wind farm. Hence, 200 PMSGs are divided into three groups. There are 75 PMSGs in the first and second group respectively. The third group is comprised of 50 PMSGs. Three different sets of typical parameters are adopted by the PMSGs in the three different groups. Following procedure is applied to examine the stability of the wind farm by using the proposed method of reduced-order modal computation.

First, a PMSG in each of three groups is selected to represent all the 200 PMSGs respectively. Oscillation modes of the wind farm are calculated by using the method of reduced-order modal computation successively with the representative PMSG from each of three groups separately. Hence, the proposed method in fact is applied for three times. All the computational results of applying the proposed method by selecting the representative PMSG from each group consecutively are used to assess the stability of the wind farm. Since the oscillation

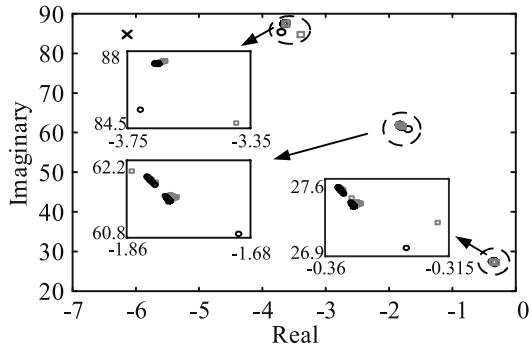

Fig. 8. Oscillation modes of the wind farm associated with DC voltage control outer loops of the GSCs when three different typical parameters of PMSGs are adopted.

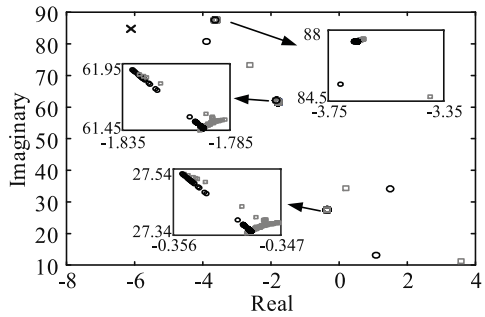

Fig. 9. Oscillation modes of the wind farm associated with DC voltage control outer loops of the GSCs when three different typical parameters of PMSGs are adopted after geographical area of wind farm is increased by 1.6 times.

TABLE IV
THREE MOST LIGHTLY DAMPED OSCILLATION MODES IN EACH OF CLUSTERS IN Fig. 8

Similar model used	Full-order model used	Error
-0.331+j26.977	-0.319+j27.204	0.84%
-0.350+j27.352	-0.347+j27.378	0.10%
-0.350+j27.352	-0.347+j27.378	0.10%
-1.697+j60.868	-1.787+j61.531	1.09%
-1.797+j61.465	-1.789+j61.529	0.10%
-1.797+j61.465	-1.789+j61.527	0.10%
-3.708+j85.343	-3.396+j84.729	0.81%
-3.649+j87.429	-3.628+j87.561	0.15%
-3.649+j87.429	-3.628+j87.560	0.15%

TABLE V
THREE MOST LIGHTLY DAMPED OSCILLATION MODES IN EACH OF CLUSTERS IN Fig. 9

Similar modal used	Full-order model used	Error
1.072+j13.157	3.562+j11.347	25.88%
-0.348+j27.374	-0.342+j27.368	0.03%
-0.348+j27.374	-0.342+j27.370	0.03%
1.502+j34.127	0.199+j34.377	3.86%
-1.788+j61.526	-1.764+j61.533	0.04%
-1.788+j61.526	-1.765+j61.535	0.04%
-3.883+j80.733	-2.627+j73.290	10.29%
-3.633+j87.540	-3.583+j87.602	0.09%
-3.633+j87.540	-3.583+j87.603	0.09%

modes associated with the DC voltage control outer loops of the GSCs are responsible for the instability of wind farm after the geographical area of wind farm is increased (see Fig. 7), they are the oscillation modes of concern. Hence, their positions on the complex plane are displayed in Fig. 8 as dark circles. It can be seen that the oscillation modes mainly distributed in three clusters on the complex plane. Due to the limitation of space, distribution of other types of oscillation modes of the wind farm on the complex plane is not presented here. However, the patterns of their distribution is as same as that shown in Fig. 8.

Second, for confirmation, oscillation modes associated with the DC voltage control outer loops of the GSCs are calculated by using the full-order model of the wind farm. They are displayed in Fig. 8 as gray rectangles. It can be seen that the oscillation modes associated with the DC voltage control outer loops of the GSCs are indeed located in three clusters on the complex plane. Reduced-order modal computation by selecting the representative PMSG consecutively can effectively cover all the results of modal computation in three clusters. Hence, the proposed method of reduced-order modal computation can be applied to assess the stability of the wind farm in the case that different typical parameters of PMSGs need to be considered in planning the grid connection. The strategy to apply the method is to select the representative PMSGs with different typical parameters separately. Successive application of the proposed method of reduced-order modal computation shall detect any possible instability risk.

Table IV presents three oscillation modes associated with the DC voltage control outer loops of the GSCs which are of the most lightly damping in each of three clusters in Fig. 8. Computational errors as compared with the results obtained from the full-order model of wind farm are also given in the last column of Table IV. It can be seen that the errors by using the proposed method of reduced-order modal computation are very small and should be completely acceptable for planning the grid connection of the wind farm.

Third, CMV method is used to derive the reduced-order model of the wind farm as an aggregated PMSG. The oscillation mode associated with the DC voltage control outer loop of the GSC is calculated and its position on the complex plane is indicated by cross in Fig. 8. It can be seen that the proposed method of reduced-order modal computation can provide more accurate stability assessment than the CMV method.

Fourth, the geographical area is increased by 1.6 times. Modal computation mentioned above is conducted again. Computational results about the oscillation modes associated with the DC voltage control outer loops of the GSCs are presented in Fig. 9. In each of three clusters of oscillation modes in Fig. 9, three most lightly damped oscillation modes are selected and presented in Table V. It can be seen that although the computational errors increase, the instability risk of the wind farm is correctly identified by the proposed method of reduced-order modal computation. However, the CMV method indicates that the wind farm is still stable, failing to detect the instability risk brought about by the increase of geographical area of the wind farm.

TABLE VI
FIVE REPRESENTATIVE PMSGS IN PLANNING THE WIND FARM

Representative PMSG-*i*	Loading condition	Parameter setting
PMSG-1	$P_0 = 0.1 p.u.$	Typical setting
PMSG-2	$15\%P_0$	Setting values reduced by 15%
PMSG-3	$15\%P_0$	Setting values increased by 15%
PMSG-4	$-15\%P_0$	Setting values reduced by 15%
PMSG-5	$-15\%P_0$	Setting values increased by 15%

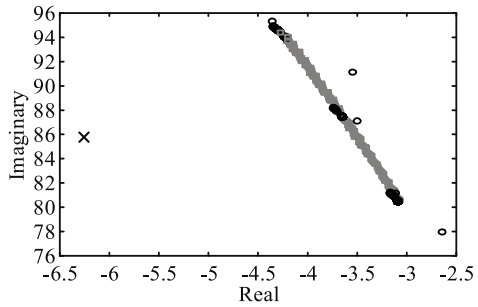

Fig. 10. Results of modal computation when variations of parameters and loading conditions of PMSGs are considered.

D. Consideration of Variations of Parameters and Loading Conditions of the PMSGs

In planning the grid connection, variations of actual parameters of the PMSGs around the typical values adopted in planning may need to be considered. In addition, changes of loading conditions of the PMSGs over the wind farm caused by the stochastic variations of wind speed may also need to be taken into account in the planning. This subsection demonstrates how the proposed method of reduced-order modal computation can be applied to accommodate those considerations in assessing the stability of the wind farm. The strategy to apply the method is similar to that adopted in the previous subsection and is introduced by the assumed planning scenarios as follows.

In planning the grid connection of the wind farm, typical loading condition of a PMSG is assumed to be 0.1 p.u., i.e., the typical active power output from the PMSG is $P_0 = 0.1$ p.u.. However, stochastic variations of wind speed over the wind farm may cause the variations of loading conditions of PMSGs within $\pm 15\% P_0$. In addition, DC voltage control outer loops of the GSCs of PMSGs may introduce instability risk to the wind farm as demonstrated in the previous subsections. Hence, the impact of setting errors in the parameters of DC voltage control outer loops of the GSCs needs to be considered. It is known that the maximum errors of parameter setting are within $\pm 15\%$ of typical setting values. Based on the above assumed scenarios and considerations for planning the wind farm, five representative PMSGs are set up as listed in Table VI.

According to Table VI, PMSG-*i* ($i = 1, 2, 3, 4, 5$) is used to represent all 200 PMSGs in the wind farm successively. Then, oscillation modes of the wind farm are calculated by using the proposed method of reduced-order modal computation. Fig. 10 displays the positions of the oscillation modes associated with the DC voltage control outer loops of the GSCs on the complex plane as hollow circles. For confirmation, the positions calculated by using the full-order model of the wind farm are displayed in Fig. 10 by gray rectangles. It can be seen that computational results from the proposed method can completely cover those obtained from the full-order model. Computational results of other types of oscillation modes of the wind farm by using the proposed method and full-order model are exactly the same. They are not displayed here due to the limitation of space. Hence, the proposed method of reduced-order modal computation can be applied to assess the stability of the wind farm when the variations of parameters and loading conditions of PMSGs need to be considered. In Fig. 10, position marked by cross is the oscillation mode calculated by using the CMV method. It can be seen that the proposed method of reduced-order modal computation is more accurate than the CMV method.

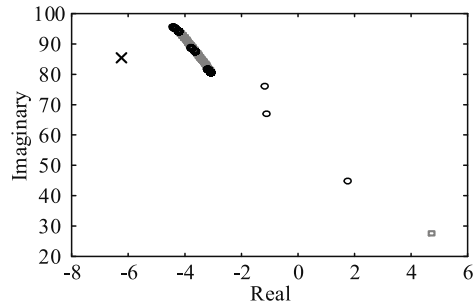

Fig. 11. Results of modal computation after the geographical area of wind farm is increased by 1.6 times when variations of parameters and loading conditions of PMSGs are considered.

After the geographical area of the wind farm is increased by 1.6 times, modal computation is conducted once more to examine the impact of variations of parameters and loading conditions of PMSGs. Fig. 11 just displays the computational results of the oscillation modes associated with the DC voltage control outer loops of the GSCs. It can be seen that the instability risk is well detected by the proposed method of reduced-order modal computation, but missed out by the CMV method.

VI. CONCLUSION

In planning the grid connection of a wind farm, the small-signal stability of the wind farm needs to be assessed to ensure that as a standalone system, the wind farm is stable. However, for a large-scale wind farm with a great number of WTGs, the dimension of state matrix of the wind farm may become too high for the modal computation due to the numerical difficulty. Hence, a method of reduced-order modal computation for the large-scale wind farm is proposed and evaluated in the paper.

Proposal of the method of reduced-order modal computation is based on the feature of the wind farm that the WTGs are arranged in radial connection for power collection. When the wind farm is planned for the grid connection, typical parameters and operating condition of the WTGs are normally used. Hence, it can be assumed that the state-space models of individual WTGs are same. Based on the assumption, this study has found that the full-order state matrix of the wind farm is of particular structure,

which can be described by a structure matrix. By calculating the eigenvalues of structure matrix, the full-order state matrix of the wind farm is proved to be similar to a diagonal block matrix. Thus, it is proposed in the paper that the modal computation of the wind farm is conducted by calculating the eigenvalues of structure matrix and the diagonal element matrices of the diagonal block matrix. Subsequently, the dimension of matrices involved in the modal computation is considerably reduced to the number of WTGs in the wind farm and the order of dynamic model of an individual WTG.

Example wind farms are presented in the paper to demonstrate and evaluate the proposed method of reduced-order modal computation. Results of evaluation indicate that although state-space models of individual WTGs may be different in the example wind farms, the proposed method of reduced-order modal computation is effective to assess the small-signal stability of the wind farms.

APPENDIX A
PROOF OF SIMILARITY TRANSFORMATION OF STATE MATRIX OF THE WIND FARM WITH M WTGS

Denote $\lambda_k, k = 1, 2, \ldots, m$ as the eigenvalues of $\boldsymbol{C}_{wm}$. There exists a matrix $\boldsymbol{P}_m$ such that

$$\boldsymbol{P}_m \boldsymbol{C}_{wm} {\boldsymbol{P}_m}^{-1} = diag(\lambda_k) \tag{A1}$$

where $\boldsymbol{C}_{wm} \in R^{m\times m}, \boldsymbol{P}_m \in R^{m\times m}, {\boldsymbol{P}_m}^{-1} \in R^{m\times m}, diag(\lambda_k) \in R^{m\times m}$.

Let

$$\boldsymbol{P}_m = \begin{bmatrix} p_{11} & p_{12} & \cdots & p_{1m} \\ p_{21} & p_{22} & \cdots & p_{2m} \\ \vdots & \vdots & \ddots & \vdots \\ p_{m1} & p_{m2} & \cdots & p_{mm} \end{bmatrix}, {\boldsymbol{P}_m}^{-1} = \begin{bmatrix} v_{11} & v_{12} & \cdots & v_{1m} \\ v_{21} & v_{22} & \cdots & v_{2m} \\ \vdots & \vdots & \ddots & \vdots \\ v_{m1} & v_{m2} & \cdots & v_{mm} \end{bmatrix} \tag{A2}$$

It can have

$$\begin{aligned} \boldsymbol{P}_m {\boldsymbol{P}_m}^{-1} &= \begin{bmatrix} p_{11} & p_{12} & \cdots & p_{1m} \\ p_{21} & p_{22} & \cdots & p_{2m} \\ \vdots & \vdots & \ddots & \vdots \\ p_{m1} & p_{m2} & \cdots & p_{mm} \end{bmatrix} \begin{bmatrix} v_{11} & v_{12} & \cdots & v_{1m} \\ v_{21} & v_{22} & \cdots & v_{2m} \\ \vdots & \vdots & \ddots & \vdots \\ v_{m1} & v_{m2} & \cdots & v_{mm} \end{bmatrix} \\ &= \begin{bmatrix} 1 & & & \\ & 1 & & \\ & & \ddots & \\ & & & 1 \end{bmatrix} = \boldsymbol{I} \in R^{m\times m} \end{aligned} \tag{A3}$$

Define following similarity transformation matrix

$$\boldsymbol{P}_{mn} = \begin{bmatrix} p_{11}\boldsymbol{I} & p_{12}\boldsymbol{I} & \cdots & p_{1m}\boldsymbol{I} \\ p_{21}\boldsymbol{I} & p_{22}\boldsymbol{I} & \cdots & p_{2m}\boldsymbol{I} \\ \vdots & \vdots & \ddots & \vdots \\ p_{m1}\boldsymbol{I} & p_{m2}\boldsymbol{I} & \cdots & p_{mm}\boldsymbol{I} \end{bmatrix},$$

$${\boldsymbol{P}_{mn}}^{-1} = \begin{bmatrix} v_{11}\boldsymbol{I} & v_{12}\boldsymbol{I} & \cdots & v_{1\mathrm{m}}\boldsymbol{I} \\ v_{21}\boldsymbol{I} & v_{22}\boldsymbol{I} & \cdots & v_{2m}\boldsymbol{I} \\ \vdots & \vdots & \ddots & \vdots \\ v_{m1}\boldsymbol{I} & v_{m2}\boldsymbol{I} & \cdots & v_{mm}\boldsymbol{I} \end{bmatrix} \tag{A4}$$

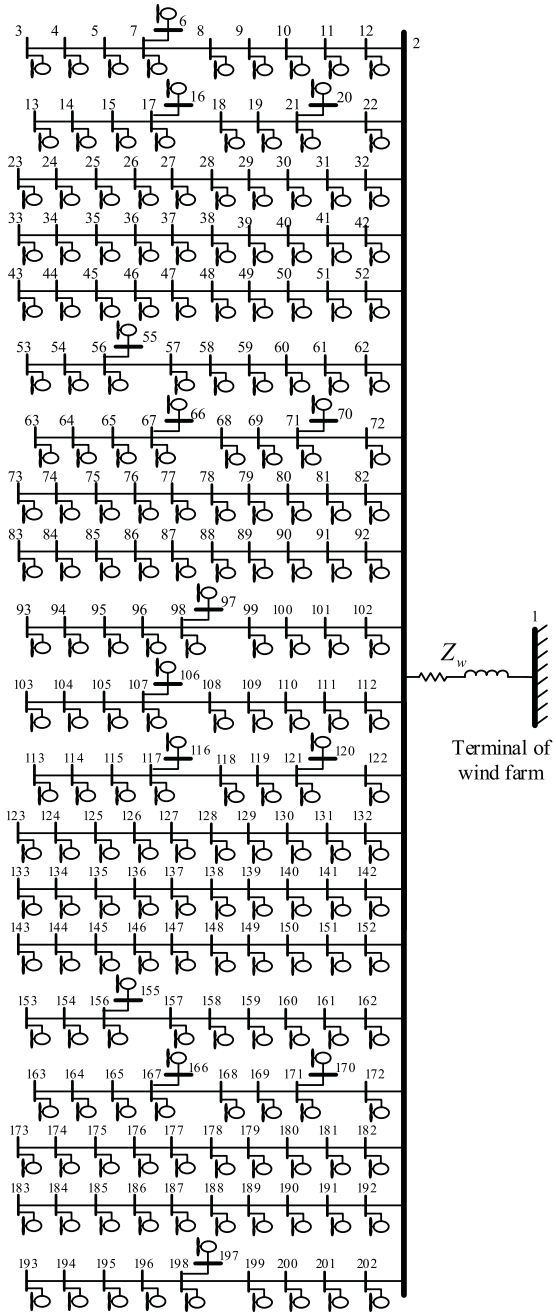

Fig. 12. Configuration of wind farm with 200 PMSGs.

where $\boldsymbol{P}_{mn} \in R^{mn\times mn}, {\boldsymbol{P}_{mn}}^{-1} \in R^{mn\times mn}$. It can easily be proved from (A3) that

$$\boldsymbol{P}_{mn} {\boldsymbol{P}_{mn}}^{-1} = diag\,[\boldsymbol{I}] \in R^{mn\times mn} \tag{A5}$$

In addition,

$$\begin{bmatrix} p_{11}\boldsymbol{I} & p_{12}\boldsymbol{I} & \cdots & p_{1m}\boldsymbol{I} \\ p_{21}\boldsymbol{I} & p_{22}\boldsymbol{I} & \cdots & p_{2m}\boldsymbol{I} \\ \vdots & \vdots & \ddots & \vdots \\ p_{m1}\boldsymbol{I} & p_{m2}\boldsymbol{I} & \cdots & p_{mm}\boldsymbol{I} \end{bmatrix} diag\,[\boldsymbol{A}_p] \begin{bmatrix} v_{11}\boldsymbol{I} & v_{12}\boldsymbol{I} & \cdots & v_{1\mathrm{m}}\boldsymbol{I} \\ v_{21}\boldsymbol{I} & v_{22}\boldsymbol{I} & \cdots & v_{2m}\boldsymbol{I} \\ \vdots & \vdots & \ddots & \vdots \\ v_{m1}\boldsymbol{I} & v_{m2}\boldsymbol{I} & \cdots & v_{mm}\boldsymbol{I} \end{bmatrix}$$

TABLE VII
CABLE LENGTH (km)

cable	L	cable	L	cable	L	cable	L
3-4	0.75	4-5	0.6	5-7	0.65	6-7	0.8
7-8	0.6	8-9	0.7	9-10	0.55	10-11	0.6
11-12	0.75	12-2	0.6	13-14	0.65	14-15	0.5
15-17	0.7	16-17	0.75	17-18	0.75	18-19	0.6
19-21	0.55	20-21	0.5	21-22	0.6	22-2	0.8
23-24	0.66	24-25	0.6	25-26	0.7	26-27	0.65
27-28	0.75	28-29	0.7	29-30	0.75	30-31	0.55
31-32	0.55	32-2	0.55	33-34	0.6	34-35	0.6
35-36	0.65	36-37	0.6	37-38	0.75	38-39	0.75
39-40	0.6	40-41	0.75	41-42	0.65	42-2	0.8
43-44	0.5	44-45	0.5	45-46	0.7	46-47	0.7
47-48	0.65	48-49	0.8	49-50	0.6	50-51	0.7
51-52	0.75	52-2	0.65	53-54	0.7	54-56	0.6
55-56	0.5	56-57	0.6	57-58	0.6	58-59	0.8
59-60	0.6	60-61	0.5	61-62	0.5	62-2	0.6
63-64	0.75	64-65	0.65	65-67	0.6	66-67	0.6
67-68	0.6	68-69	0.6	69-71	0.5	70-71	0.55
71-72	0.65	72-2	0.5	73-74	0.75	74-75	0.8
75-76	0.65	76-77	0.6	77-78	0.5	78-79	0.6
79-80	0.55	80-81	0.75	81-82	0.65	82-2	0.7
83-84	0.6	84-85	0.5	85-86	0.65	86-87	0.7
87-88	0.7	88-89	0.65	89-90	0.5	90-91	0.6
91-92	0.5	92-2	0.6	93-94	0.6	94-95	0.75
95-96	0.7	96-98	0.5	97-98	0.7	98-99	0.5
99-100	0.5	100-101	0.65	101-102	0.7	102-2	0.8
103-104	0.55	104-105	0.7	105-107	0.75	106-107	0.6
107-108	0.8	108-109	0.75	109-110	0.5	110-111	0.8
111-112	0.65	112-2	0.5	113-114	0.6	114-115	0.55
115-117	0.8	116-117	0.65	117-118	0.7	118-119	0.65
119-121	0.75	120-121	0.5	121-122	0.5	122-2	0.7
123-124	0.76	124-125	0.6	125-126	0.6	126-127	0.6
127-128	0.75	128-129	0.75	129-130	0.7	130-131	0.6
131-132	0.5	132-2	0.6	133-134	0.65	134-135	0.5
135-136	0.6	136-137	0.7	137-138	0.7	138-139	0.75
139-140	0.65	140-141	0.7	141-142	0.65	142-2	0.85
143-144	0.55	144-145	0.5	145-146	0.65	146-147	0.75
147-148	0.6	148-149	0.75	149-150	0.65	150-151	0.8
151-152	0.65	152-2	0.65	153-154	0.6	154-156	0.7
155-156	0.6	156-157	0.5	157-158	0.65	158-159	0.75
159-160	0.5	160-161	0.6	161-162	0.55	162-2	0.55
163-164	0.65	164-165	0.75	165-167	0.55	166-167	0.65
167-168	0.8	168-169	0.5	169-171	0.5	170-171	0.55
171-172	0.55	172-2	0.5	173-174	0.75	174-175	0.6
175-176	0.65	176-177	0.7	177-178	0.55	178-179	0.6
179-180	0.65	180-181	0.7	181-182	0.7	182-2	0.65
183-184	0.65	184-185	0.5	185-186	0.6	186-187	0.7
187-188	0.75	188-189	0.65	189-190	0.5	190-191	0.6
191-192	0.5	192-2	0.7	193-194	0.6	194-195	0.7
195-196	0.7	196-198	0.55	197-198	0.7	198-199	0.6
199-200	0.5	200-201	0.65	201-202	0.65	202-2	0.8
2-1	1						

$$= diag\left[\boldsymbol{A}_p\right]\begin{bmatrix} p_{11}\boldsymbol{I} & p_{12}\boldsymbol{I} & \cdots & p_{1m}\boldsymbol{I} \\ p_{21}\boldsymbol{I} & p_{22}\boldsymbol{I} & \cdots & p_{2m}\boldsymbol{I} \\ \vdots & \vdots & \ddots & \vdots \\ p_{m1}\boldsymbol{I} & p_{m2}\boldsymbol{I} & \cdots & p_{mm}\boldsymbol{I} \end{bmatrix}$$

$$\times \begin{bmatrix} v_{11}\boldsymbol{I} & v_{12}\boldsymbol{I} & \cdots & v_{1\mathrm{m}}\boldsymbol{I} \\ v_{21}\boldsymbol{I} & v_{22}\boldsymbol{I} & \cdots & v_{2m}\boldsymbol{I} \\ \vdots & \vdots & \ddots & \vdots \\ v_{m1}\boldsymbol{I} & v_{m2}\boldsymbol{I} & \cdots & v_{mm}\boldsymbol{I} \end{bmatrix} = diag\left[\boldsymbol{A}_p\right] \tag{A6}$$

From (A1),

$$\begin{bmatrix} p_{11}\boldsymbol{I} & p_{12}\boldsymbol{I} & \cdots & p_{1m}\boldsymbol{I} \\ p_{21}\boldsymbol{I} & p_{22}\boldsymbol{I} & \cdots & p_{2m}\boldsymbol{I} \\ \vdots & \vdots & \ddots & \vdots \\ p_{m1}\boldsymbol{I} & p_{m2}\boldsymbol{I} & \cdots & p_{mm}\boldsymbol{I} \end{bmatrix}\begin{bmatrix} c_{11}\boldsymbol{I} & c_{12}\boldsymbol{I} & \cdots & c_{1m}\boldsymbol{I} \\ c_{21}\boldsymbol{I} & c_{22}\boldsymbol{I} & \cdots & c_{2m}\boldsymbol{I} \\ \vdots & \vdots & \ddots & \vdots \\ c_{m1}\boldsymbol{I} & c_{m2}\boldsymbol{I} & \cdots & c_{mm}\boldsymbol{I} \end{bmatrix}$$

$$diag\left[\boldsymbol{B}_P\boldsymbol{Z}_C\boldsymbol{C}_P\right]\begin{bmatrix} v_{11}\boldsymbol{I} & v_{12}\boldsymbol{I} & \cdots & v_{1\mathrm{m}}\boldsymbol{I} \\ v_{21}\boldsymbol{I} & v_{22}\boldsymbol{I} & \cdots & v_{2m}\boldsymbol{I} \\ \vdots & \vdots & \ddots & \vdots \\ v_{m1}\boldsymbol{I} & v_{m2}\boldsymbol{I} & \cdots & v_{mm}\boldsymbol{I} \end{bmatrix}$$

$$= \begin{bmatrix} p_{11}\boldsymbol{I} & p_{12}\boldsymbol{I} & \cdots & p_{1m}\boldsymbol{I} \\ p_{21}\boldsymbol{I} & p_{22}\boldsymbol{I} & \cdots & p_{2m}\boldsymbol{I} \\ \vdots & \vdots & \ddots & \vdots \\ p_{m1}\boldsymbol{I} & p_{m2}\boldsymbol{I} & \cdots & p_{mm}\boldsymbol{I} \end{bmatrix}\begin{bmatrix} c_{11}\boldsymbol{I} & c_{12}\boldsymbol{I} & \cdots & c_{1m}\boldsymbol{I} \\ c_{21}\boldsymbol{I} & c_{22}\boldsymbol{I} & \cdots & c_{2m}\boldsymbol{I} \\ \vdots & \vdots & \ddots & \vdots \\ c_{m1}\boldsymbol{I} & c_{m2}\boldsymbol{I} & \cdots & c_{mm}\boldsymbol{I} \end{bmatrix}$$

$$\times \begin{bmatrix} v_{11}\boldsymbol{I} & v_{12}\boldsymbol{I} & \cdots & v_{1\mathrm{m}}\boldsymbol{I} \\ v_{21}\boldsymbol{I} & v_{22}\boldsymbol{I} & \cdots & v_{2m}\boldsymbol{I} \\ \vdots & \vdots & \ddots & \vdots \\ v_{m1}\boldsymbol{I} & v_{m2}\boldsymbol{I} & \cdots & v_{mm}\boldsymbol{I} \end{bmatrix} diag\left[\boldsymbol{B}_P\boldsymbol{Z}_C\boldsymbol{C}_P\right]$$

$$= diag\left[\lambda_k\boldsymbol{I}\right] diag\left[\boldsymbol{B}_P\boldsymbol{Z}_1\boldsymbol{C}_P\right] = diag\left[\lambda_k\boldsymbol{B}_P\boldsymbol{Z}_C\boldsymbol{C}_P\right] \tag{A7}$$

From (16), (A6) and (A7),

$$\boldsymbol{P}_{mn}\boldsymbol{A}_w{\boldsymbol{P}_{mn}}^{-1} = diag\left[\boldsymbol{A}_p + \lambda_k\boldsymbol{B}_P\boldsymbol{Z}_C\boldsymbol{C}_P\right] \tag{A8}$$

Hence, state matrix of the wind farm, $\boldsymbol{A}_w$, is similar to $diag[\boldsymbol{A}_p + \lambda_k\boldsymbol{B}_P\boldsymbol{Z}_C\boldsymbol{C}_P]$.

APPENDIX B
CABLE PARAMETERS AND THE CONFIGURATION OF THE LARGE-SCALE WIND FARM WITH 200 PMSGS

Configuration of wind farm with 200 PMSGs is shown in Fig. 12. Lengthes of cables are given in Table VII, where $i-j, (i, j = 1, 2, \ldots, 202)$ denotes the cable between node *i* and *j*. Impedance of cable/per km. is $Z_C = 0.0175 + j0.0367$.

REFERENCES

[1] Y. Wu, C. Lee, and S.-H. Tsai, "Onshore wind farm planning and system simulation analysis under low-carbon-island project at Penghu," in *Proc. 16th Int. Conf. Intell. Syst. Appl. Power Syst.*, 2011, pp. 1–7.

[2] H. Zhao *et al.*, "New type of wind farm planning method research," in *Proc. 2nd IET Renewable. Power Gener.*, 2013, pp. 1–4.

[3] W. Liu, Y. Wu, C. Lee, and C. Chen, "Effect of low-voltage-ride-through technologies on the first Taiwan offshore wind farm planning," *IEEE Trans. Sustain. Energy*, vol. 2, no. 1, pp. 78–86, Oct. 2010.

[4] A. Moharana, R. K. Varma, and R. Seethapathy, "Modal analysis of type-1 wind farm connected to series compensated transmission line and LCC HVDC transmission line," in *Proc. IEEE Elect. Power Energy Conf.*, 2012, pp. 202–209.

[5] N. N. Shah and S. R. Joshi, "Small signal stability analysis of DFIG based wind farms connected to SMIB," in *Proc. Int. Conf. Smart Grids, Power Adv. Control Eng.*, 2017, pp. 247–252.

[6] R. Wang *et al.*, "Small signal stability analysis with high penetration of grid-connected wind farm of PMSG type considering the weak effect," in *Proc. IEEE PES General Meeting*, 2014, pp. 1–5.

[7] Y. Pan, S. Mei, F. Liu, W. Wei, C. Shen, and J. Wei, "Admissible region of large-scale uncertain wind generation considering small-signal stability of power system," *IEEE Trans. Sustain. Energy*, vol. 7, no. 4, pp. 1611–1623, May 2016.

[8] W. Du, X. Chen, and H. Wang, "Power system electromechanical oscillation modes as affected by dynamic interactions from grid-connected PMSGs for wind power generation," *IEEE Trans. Sustain. Energy*, vol. 8, no. 3, pp. 1301–1312, Mar. 2017.

[9] K. Givaki and L. Xu, "Stability analysis of large wind farms connected to weak AC networks incorporating PLL dynamics," in *Proc. Renewable Power Gener.*, 2015, pp. 1–6.

[10] Y. Wang *et al.*, "Comprehensive modeling and parameter identification of wind farms based on wide-area measurement systems," *J. Mod. Power Syst. Clean Energy*, vol. 4, no. 3, pp. 383–393, 2016.
[11] M. Ali *et al.*, "Probabilistic clustering of wind generator," in *Proc. IEEE PES General Meeting*, Providence, RI, USA, Jul. 2010, pp. 1–6.
[12] J. Zou, C. Peng, H. Xu, and Y. Yan, "A fuzzy clustering algorithm-based dynamic equivalent modeling method for wind farm with DFIG," *IEEE Trans. Energy Convers.*, vol. 30, no. 4, pp. 1329–1337, May 2015.
[13] Y Zhou, L Zhao, and W Lee, "Robustness analysis of dynamic equivalent model of DFIG wind farm for stability study," *IEEE Trans. Ind. Appl.*, vol. 54, no. 6, pp. 5682–5690, Nov. 2018.
[14] M. El-Sharkawi, "Dynamic equivalent models for wind power plants," in *Proc. IEEE Power Energy Soc. General Meeting*, Detroit, MI, USA, Jul. 2011, pp. 1–5.
[15] I. Erlich *et al.*, "Determination of dynamic wind farm equivalents using heuristic optimization," in *Proc. IEEE PES General Meeting*, San Diego, CA, USA, Jul. 2012, pp. 1–8.
[16] P. Wang, Z. Zhang, Q. Huang, N. Wang, X. Huang, and Z. Zhang, "Improved wind farm aggregated modeling method for large-scale power system stability studies," *IEEE Trans. Power Syst.*, vol. 33, no. 6, pp. 6332–6342, Nov. 2018.
[17] D. H. R. Suriyaarachchi, U. D. Annakkage, C. Karawita, and U. D. Annakkage, "A procedure to study sub-synchronous interactions in wind integrated power system," *IEEE Trans. Power Syst.*, vol. 28, no. 1, pp. 377–384, Jul. 2012.
[18] L. P. Kunjumuhammed, B. C. Pal, C. Oates, and K. J. Dyke, "Electrical oscillations in wind farm systems: Analysis and insight based on detailed modeling," *IEEE Trans. Sustain. Energy*, vol. 7, no. 1, pp. 51–62, Jan. 2016.
[19] D. Stet *et al.*, "Numerical modelling of a wind farm located in the south area of Romania through equivalent electrical circuits," in *Proc. 49th Int. Univ. Power Eng. Conf.*, 2014, pp. 1–4.
[20] S. Li, T. A. Haskew, R. P. Swatloski, and W. Gathings, "Optimal and direct-current vector control of direct-driven PMSG wind turbine," *IEEE Trans. Power Electro.*, vol. 27, no. 5, pp. 2325–2337, May 2012.
[21] W. Li, P. Chao, X. Liang, D. Xu, and X. Jin, "An improved single-machine equivalent method of wind power plants by calibrating power recovery behaviors," *IEEE Trans. Power Syst.*, vol. 33, no. 4, pp. 4371–4381, Jul. 2018.
[22] J. Brochu, C. Larose, and R. Gannon. "Generic equivalent collector system parameters for large wind power plants," *IEEE Trans. Energy Convers.*, vol. 26, no. 2, pp. 542–549, Jun. 2011.

Authors' photographs and biographies not available at the time of publication.